The 9th European Congress on Computational Methods in Applied Sciences and Engineering
ECCOMAS Congress 2024
3 – 7 June 2024, Lisboa, Portugal

PHASE FIELD MODELLING OF CUCRZR ALLOY FOR NUCLEAR FUSION

Daniel Kell* and Thomas Haynes*

*School of Engineering
University of East Anglia (UEA**)**, Norwich, NR4 7TJ, UK
E-mail: D.Kell@uea.ac.uk

Key words: CuCrZr; Pitting Corrosion; Divertor; Phase Field Model; Nuclear Fusion

ABSTRACT

A fusion reactor produces energy by harnessing the process of nuclear fusion. This process involves the combination of hydrogen isotopes (deuterium and tritium) to form helium plasma at extremely high temperatures. An example of a nuclear fusion reactor is the Spherical Tokomak for Energy Production (STEP) reactor. The divertor is a section within the fusion reactor that dissipates heat energy from the core using a series of monoblocks that form a matrix of pipes that involve water coolant flowing through them. CuCrZr is a potential alloy for use in the divertor system in reactors such as STEP due to its beneficial mechanical properties such as high strength and thermal conductivity at increased temperatures. The main disadvantage of CuCrZr is that when the alloy is being used for extended periods of time above temperatures of 570 K, the alloy has a reduction in strength due to irradiation which then makes it vulnerable to embrittlement and consequently structural damage.

This paper presents an overview the corrosion and fracture performance of a representative section of a divertor monoblock for the STEP reactor. Both corrosion and fracture are modelled using phase field modelling, implemented in the commercial software 'COMSOL Multiphysics'. Using COMSOL, a model for a single monoblock that makes up the divertor system is used in two studies: one to determine the impact of corrosion on the CuCrZr material, and the second to determine the impact upon the structure of this corrosion.

For the corrosion study, pure copper was a surrogate material, and its electro-chemical properties were used to replace CuCrZr in the monoblock. The parameters used for the corrosion study included current density, diffusion coefficient and equilibrium potential. This study was used to identify the effect of pitting corrosion in the divertor and the conditions, such as the Tafel slope, that initiate and accelerate this process. Following on from the corrosion studies, an investigation was conducted which involved the analysis of the load the CuCrZr material and the monoblock can withstand during a simulation in which the size of the pit expanded within the total time of 365 days. The corrosion rate gained from changing the pH level of the electrolyte indicates a transition region at pH 6. This transition region is the result of protective oxide film breaking down on the surface of the CuCrZr ring. The development of the brittle fracture study and the phase field model show that CuCrZr is susceptible towards pitting corrosion and structural degradation due the oxide deposits within the pit that causes volumetric expansion leading to crack propagation. At the interface between materials, the crack is deflected due to the dissimilar materials having a difference in Griffiths energy release rate values.

1 INTRODUCTION

1.1 STEP

The Spherical Tokomak for Energy Production (STEP) reactor is a nuclear fusion reactor that is shaped like an ‘apple core’ (as shown in Figure 1) which uses different isotopes of hydrogen (deuterium and tritium) gases to produce plasma at extremely high temperatures which produces a helium nucleus and a neutron [1], [2].

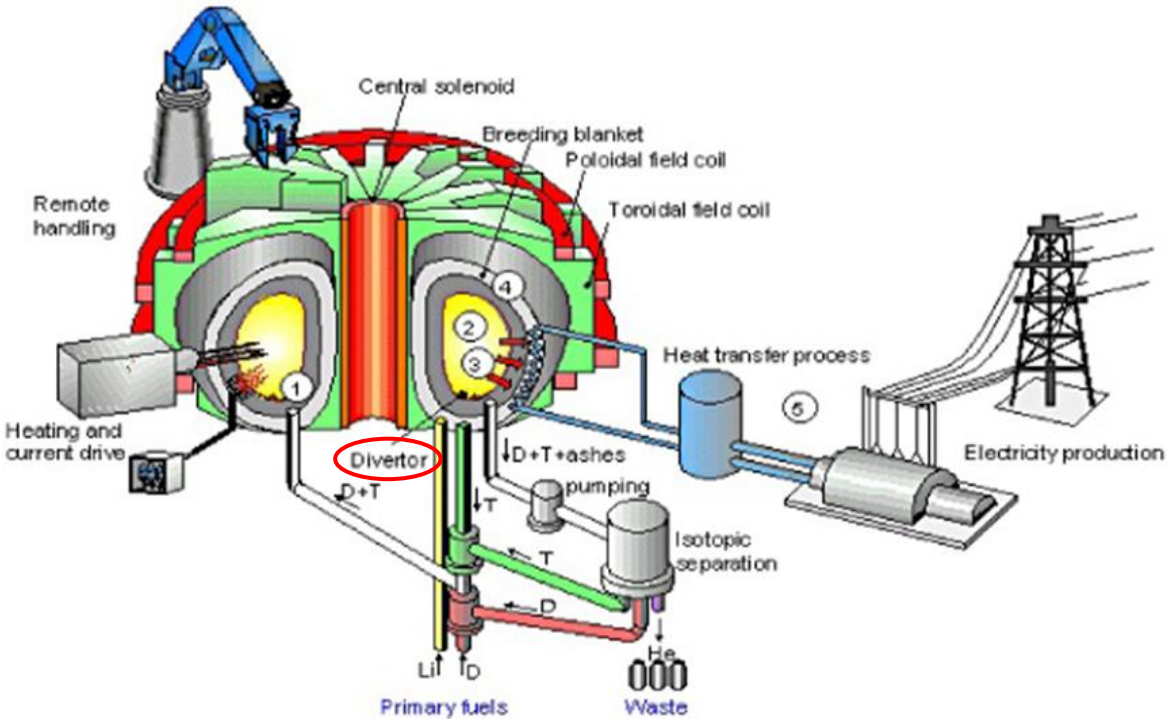

Figure 1: Design for a generic magnetic confinement reactor produced from Figure 3 in [3].

This plasma is then held in place with strong magnets that surround the core in a tokomak design which is essentially a doughnut-shaped chamber. One issue in the STEP reactor is that the plasma will be operating at over 150 million Kelvin, therefore, the reactor will need to have thermal and neutron radiation shielding to protect the magnetic coils, the central column within the reactor and the pressure vessels [4], [5]. The neutrons that interact with materials and cause irradiation are mainly fast neutrons within the neutron flux of the reactor. These then cause effects to surrounding materials such as ionisation, nuclear transmutation, phase transmutation and displacement damage effects [6]. These effects can cause changes to the microstructure of the material which causes problems such as embrittlement, leading to a reduction in the material’s operational life [7].

The divertor (highlighted in Figure 1) allows the temperatures in the reactor core to be controlled. As shown in Figure 2, the divertor is made up of a matrix of passages that have a constant flow of water coolant going through them. The divertors is located within the core of a tokomak reactor and is oriented to be facing the plasma generated from the nuclear fusion reaction. This provides temperatures of up to 873 Kelvin on to the plasma facing materials on the divertor [8].

Figure 2: Cross-section of the divertor component from the JET reactor at Culham Centre of Fusion Energy, Oxford.

1.2 Phase Field Modelling

Phase field models are tools that accurately simulate the changes of microstructures in complex morphologies of materials [9].The models are useful when the materials studied consist of complex alloys which contain secondary or tertiary species [10]. As phase field modelling is an implicit method, complicated morphologies can be readily generalized in any dimension especially when dealing with problems with electrochemical reactions and mechanical deformations [10].

1.3 Copper Chromium Zirconium

Copper chromium zirconium (CuCrZr) is a copper alloy containing a tertiary species. Due to its combination of metals, it provides elevated levels of electrical conductivity and mechanical properties at high temperatures [11], [12]. These properties allowed CuCrZr to be considered to be used in plasma facing applications and divertor plates used in nuclear fusion reactors such as Joint European Torus (JET) or STEP [13], [14].

1.4 Pitting Corrosion

Pitting corrosion is the chemical process of the formation of localized pits in metals that are exposed to aqueous solutions [15]. Anions from acidic solutions induce pitting corrosion due to the anions breaking away the protective film on the surface of the metal [15]. This protective fil is usually an oxide film, however, in some applications a corrosion inhibitor is provided to reduce the rate of corrosion on the metal surface [16].

2 METHODOLOGY

2.1 Theoretical background

2.1.1 Corrosion theory

The Tafel slope is part of the Tafel equation for electrochemical kinetics as shown in Equation (1). It relates to the rate of an electrochemical reaction using current density, i, and exchange current density, i_0, to the overpotential, η, where a reaction occurs in two half reactions on different electrodes [17], [18]. The Tafel equation is then applied to both electrodes. Equation (2) is the Tafel slope, reproduced from [18], in which λ is the constant value of ln (10); k_B, is Boltzmann's constant; T, is the absolute temperature and; e is the electronic charge of an electron and; α, is the inverse of the charge transfer coefficient, [18].

$$\eta = \pm A \cdot log_{10}\left(\frac{i}{i_0}\right) \tag{1}$$

$$A = \frac{\lambda k_B T}{e\alpha} \tag{2}$$

2.1.2 Brittle fracture theory

The critical energy release rate, also known as the Griffith's energy release rate, is the work required to break atomic bonds against the strain energy that is released when cracks form. Combining these topics form the Griffith's energy release rate criterion [19]. Equation (3) is the tensile stress failure denoted by σ_f, reproduced from [19], with G_c being the Griffith critical energy release rate; E, is the Young's modulus of the material and; a, is the crack length.

$$\sigma_f = \sqrt{\frac{G_c E}{\pi a}} \tag{3}$$

2.2 Assumptions

For the parameters, several assumptions were made:

- Copper metal as a surrogate for CuCrZr in the corrosion study.
- The equilibrium potential was found using the redox reactions between copper, water and oxygen as copper is unreactive to pure water and needs oxygen to initiate corrosion.
- Interpolations for corrosion study will be reproduced from the pit corrosion COMSOL example from [20].
- A plane stress model is used for the brittle fracture study due to model thickness being less than the model width dimension. The model thickness is assumed to be 1 mm to simplify the Griffith's energy release rate calculations.

2.3 CuCrZr parameters

Table 1 shows the mechanical, electrical, and material properties of CuCrZr.

Table 1 - Table of parameters for CuCrZr

Solid Mechanics Module		**Source**	**Corrosion Module (Copper values)**		**Source**
Young's modulus	136.00 [GPa]	[21]	Tafel slope	0.058 [V/decade]	Calculated using background theory
Density	8.91 [g/cm^3]	[21]	Current density	3.10x10^6 [A/m^2]	[22]
Poisson ratio	0.30	[21]	Equilibrium potential	0.061 [V]	[23]
Free surface energy	1.65 [J/m^2]	[24]	Electrical conductivity	58 [MS/m]	[23]
Griffiths energy release rate	82.50 [J/m^2]	Calculated using background theory	Exchange current density	1.00 [A/m^2]	[22]
Sigma$_f$	26.73 [MPa]	Calculated using background theory	Molar mass	63.546 [g/mol]	[23]
Specific heat capacity	370.00 [J/kgK]	[25]	Diffusion coefficient	7.33x10^{-10} [m^2/s]	[26]
Thermal conductivity	325.00 [W/mK]	[21]	pH	10	[20]
Pore saturation	0.5	[20]	Temperature	293.15 [K]	[20]
Hardness	175 [HB]	[25]			
Ultimate tensile strength	550.00 [MPa]	[21]			
Yield strength	310.00 [MPa]	[21]			
Parameter Load	0	[27]			

2.3 Model dimensions

Both studies include a 2D cross-section of the monoblock in the divertor system with dimensions from [28]. As shown in Figure 3, the dimensions of the model are a 28x28 mm square which surrounds 16 mm and 14 mm diameter rings that have a thickness of 1 mm and 1.5 mm respectively. The gap at which the water coolant will flow through is 11 mm in diameter and is positioned in the center of the model. This model consists of the materials necessary which are CuCrZr, copper and tungsten. The monoblock is made with tungsten which has two 2 mm holes punctured into it to represent the rigid connectors. The 14 mm diameter ring is made from the CuCrZr alloy, and the 16 mm diameter ring is made from copper. The initial pit has a radius of 5 μm and is situated in the CuCrZr ring. The plasma facing side is highlighted in Figure 3.

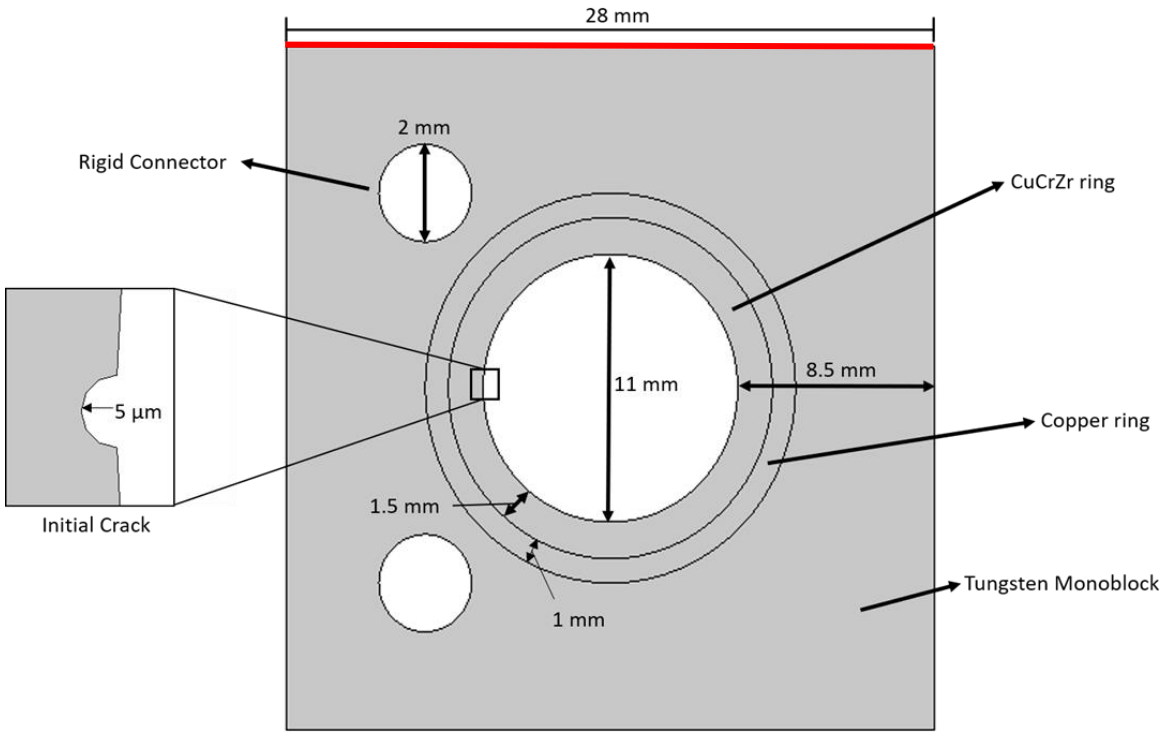

Figure 3: Dimensions for monoblock model.

2.4 Meshing and boundary conditions

A 'free quad' mesh at a predefined 'extra fine' sensitivity was used, as shown in Figure 4. Automatic remeshing is utilized to eliminate any mesh inversion. This combined with the properties of the free quad mesh reduce computational power to provide a reduction in simulation time.

The boundary conditions for the study are shown in Figure 4. The top rigid connector (highlighted in red) is assigned to displace in the positive y-direction while the bottom rigid connector has fully fixed constraints applied (highlighted in blue). The inside of the CuCrZr ring (highlighted in green) is the area where coolant is applied to determine the corrosion rate for each pH value. This involves identifying the central domain to be the electrolyte and the CuCrZr ring to be the electrode surface. The concentrations for the H^+ and OH^- ions need to be distinguished to simulate the pH of the electrolyte. The electrolyte potential also must be identified in the initial pit (highlighted in orange) to simulate the flow of electrons during pitting corrosion.

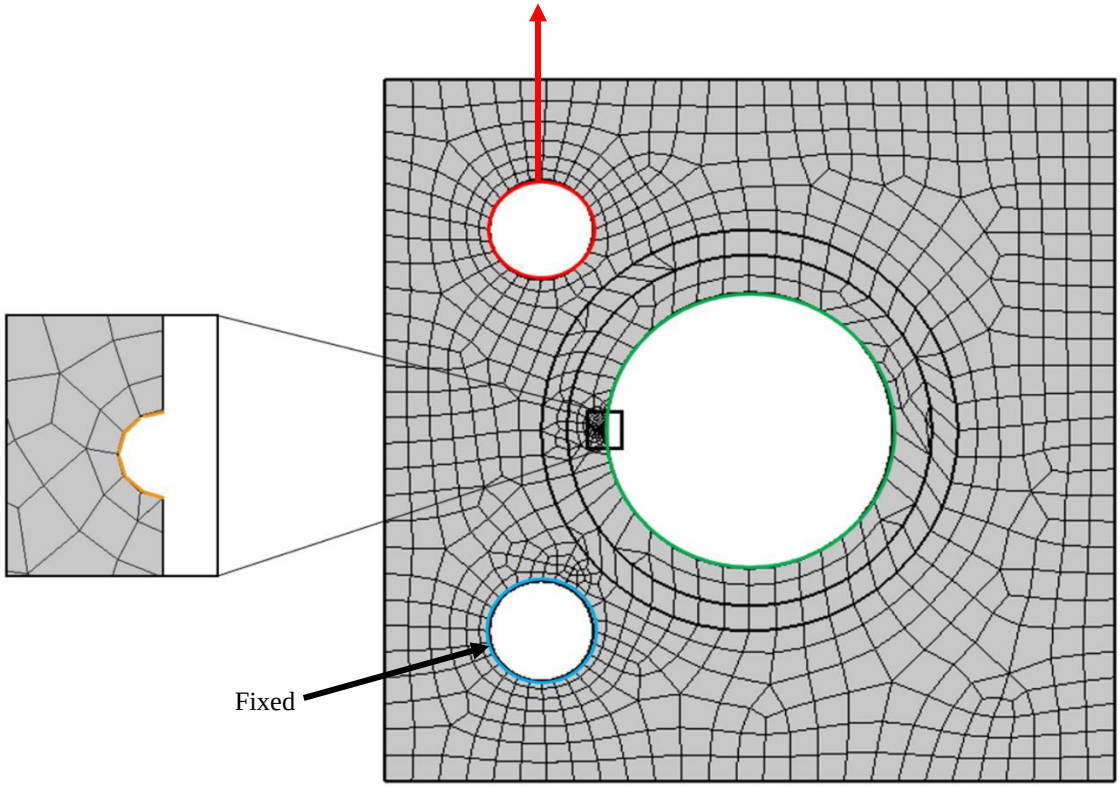

Figure 4: Mesh and boundary conditions for the monoblock model.

Once the mesh was applied to the model, stationery and time-dependent study steps were configured. For the stationary study step, the solid mechanics module was selected. For the time-dependent study step, the output times ranged from 0 to 365 days with an iteration step of 1 day.

3 RESULTS

As the pH levels vary in the coolant, the corrosion rate for the solution also changes. This relationship with corrosion rate and pH level effecting the CuCrZr ring in the monoblock is shown in Figure 5.

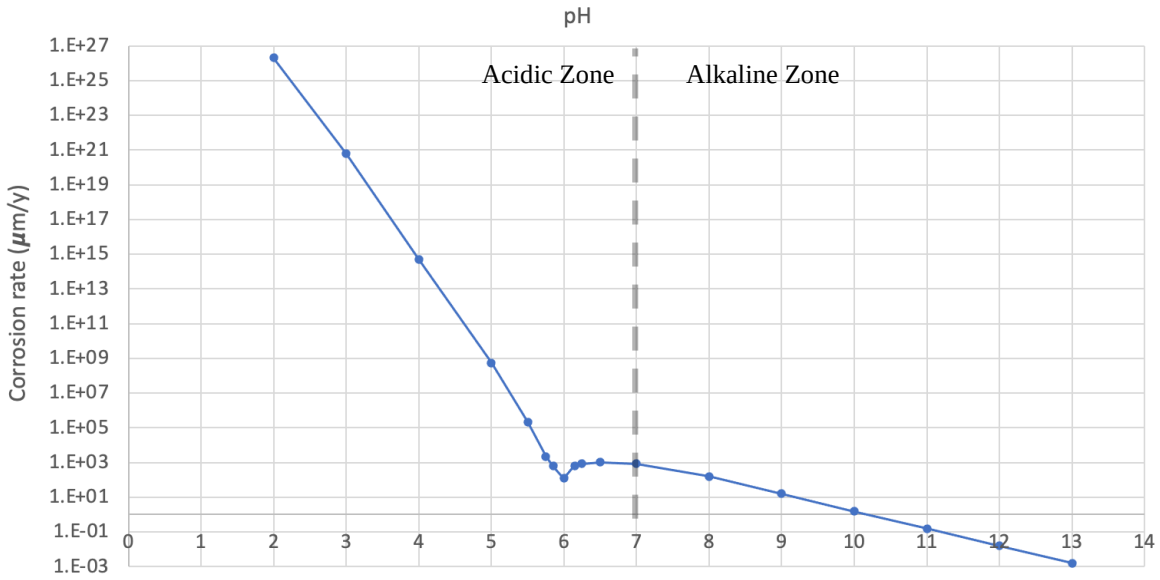

Figure 5: Plot of corrosion rate against various pH levels.

The corrosion rate at pH 5.8 to 7 is situated around 1000 μm per year. The rate gradient in the alkaline zone above pH 7 is expressed as $R_{alkaline} = 2E + 10e^{-2.3[pH]}$ and the rate gradient in the acidic zone below pH 5.8 is represented as $R_{acidic} = 2E + 38e^{-13.53[pH]}$.

The distribution of the phase field at the last iteration of the simulation for crack lengths 5 μm and 1280 μm is shown in Figure 6. The deflections in the phase field show that different materials are involved in the model. The crack on the right-hand side of the model is thinner than the crack on the left-hand side for both instances of varying crack length.

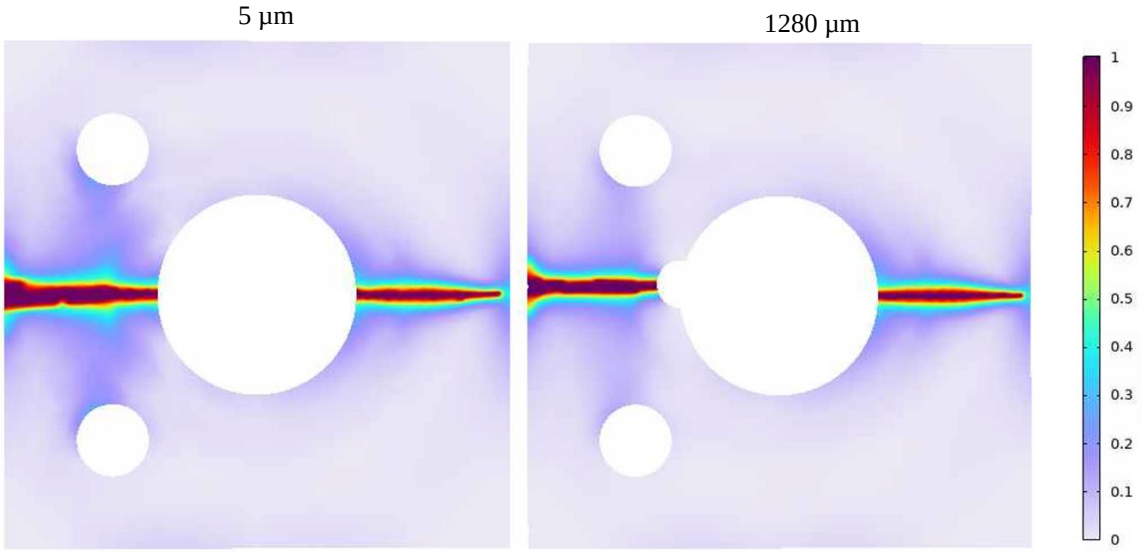

Figure 6: Comparison between crack phase field profiles at crack lengths of 5 μm and 1280 μm. The legend represents the variation of phase field.

The variation of the damage profile at the last iteration of the simulation for crack lengths 5 μm and 1280 μm is shown in Figure 7. The deflections in the damage profile show that different materials are involved in the model. The legend represents the damage variation instigated by the crack propagation.

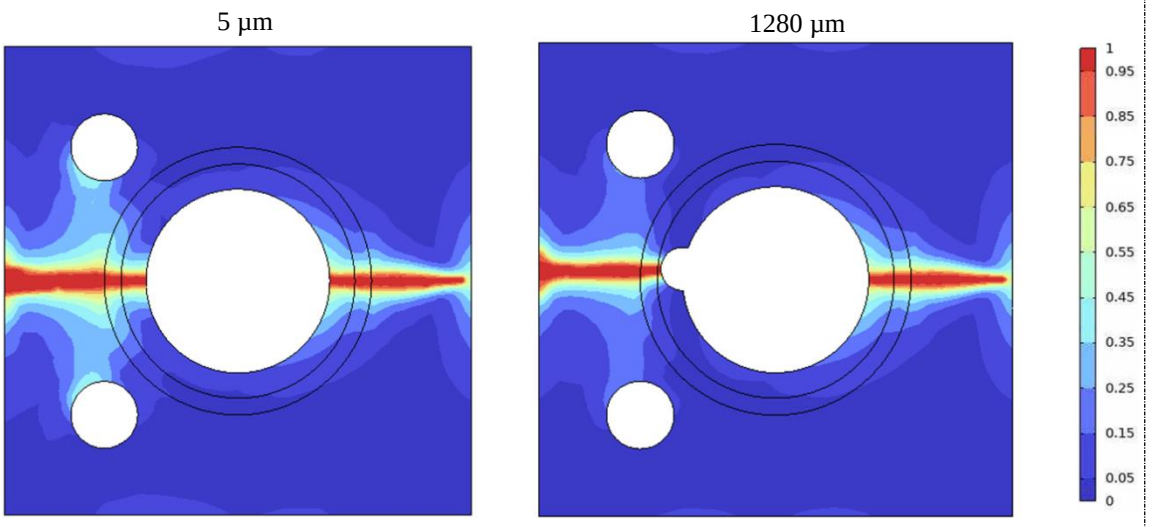

Figure 7: Damage profile comparison at crack lengths of 5 µm and 1280 µm.

The crack trajectories for differing crack lengths are shown in Figure 8. The red arrows represent the tensile forces applied to the model during simulation. The result of the tensile forces causes the coloured contours to appear which indicates the stresses that act on the model.

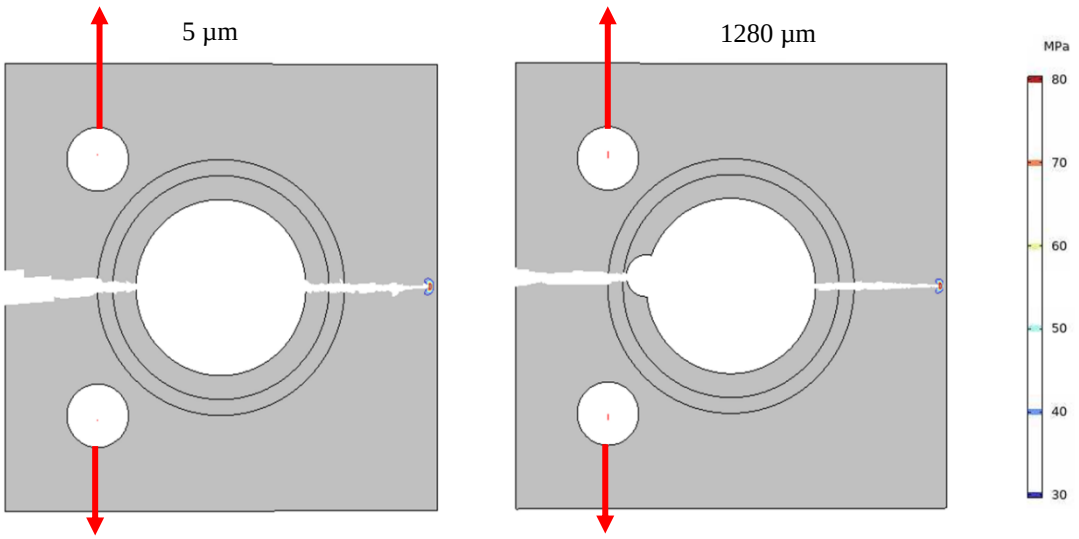

Figure 8: Comparison of the crack trajectories at crack lengths of 5 µm and 1280 µm.

Figure 9 shows the relationship between the maximum load the model undertakes at various crack lengths and crack tip radii.

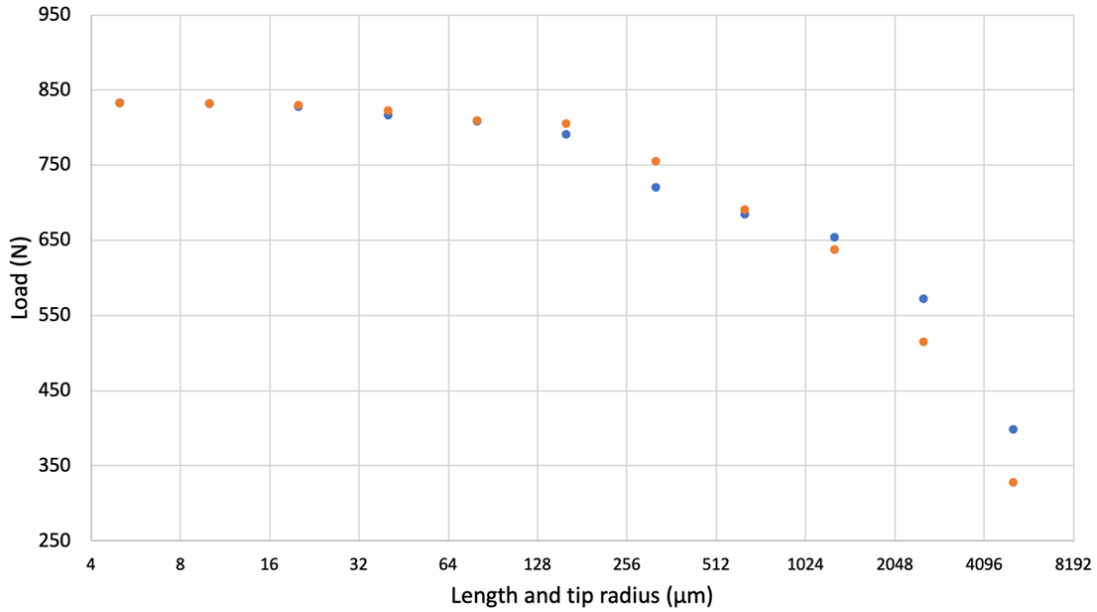

Figure 9: Plot of load against various crack lengths with the default depth and width starting at 5 µm.

4 DISCUSSION

The results indicate that as pH levels decrease below 6, the corrosion rate increases as a function of $e^{m[pH]}$ which leads to a higher probability in pitting corrosion and a growth in crack length and crack tip radius as shown in Figure 5. This is due to the influx of H+ ions in the water coolant as the coolant is irradiated by the nuclear fusion core during operation. This leads to the monoblock withstanding less load as the crack length and tip radius increases represented in Figure 9. Above pH 7, the corrosion rate varies using the function, $e^{n\{pH]}$.

This suggests that CuCrZr is susceptible to pitting corrosion at low pH levels, which in turn weakens the material due to crack propagation between the different monoblock materials. The relationship between pH and the corrosion rate is due to the radiolysis of the water coolant producing significant H^+ ions which in turn enhances pitting corrosion.

The pitting corrosion profile shows uniform pit growth in the CuCrZr ring which indicates that changing the crack tip radius in the model provides a more relevant representation of the pitting corrosion compared to changing the crack length in the model.

The deflection in the phase field model in Figure 6 and the damage profile in Figure 7 indicate the change in the material properties across each boundary of the monoblock. The main property that would cause these deflections is the Griffiths energy release rate as this determines the amount of energy needed to instigate a crack in the materials.

The corrosion rate shown in Figure 5, can be utilized to predict the pit size at any given time for a range of coolant pH levels. For example, using pH 7 water coolant within the CuCrZr pipe for the time span of one annum, the pit size is to increase by 1000 µm. This pit size can then be used to determine the maximum load CuCrZr can withstand which in turn provides a timescale for the operational life of the CuCrZr material in the monoblock system of the divertor.

5 CONCLUSION

In conclusion;

- The results indicate that CuCrZr is more susceptible to pitting corrosion at low pH levels of 5.8 to 2 that are situated in the acidic region where the rate has a gradient, m, of -13.53.
- CuCrZr is less susceptible to pitting corrosion at high pH levels of 7 to 13 that are situated in the alkaline region where the rate has a gradient, n, of -2.3.
- Combining the corrosion rate data with time and the load data, predictions can be made for the operational life of the CuCrZr ring leading to decisions to be made for maintenance of the divertor based on the pH used for the coolant of the nuclear fusion reactor. An example of this is using 7 pH water coolant within the divertor system for one annum predicts that the size of the pit will be 1000 µm. A pit size of 1000 µm is predicted to withstand 650 N applied to the CuCrZr ring.
- It is recommended that the coolant used in the divertor of the nuclear fusion reactor should have a pH value higher than pH 6 as this will minimise pitting corrosion on the CuCrZr ring in the monoblock. This will then in turn reduce maintenance on the divertor and improve operational life leading to a more efficient nuclear fusion reactor.

6 REFERENCES

[1] 'Fusion in brief - Culham Centre for Fusion Energy'. Accessed: Nov. 17, 2022. [Online]. Available: https://ccfe.ukaea.uk/fusion-energy/fusion-in-brief/

[2] 'STEP - Spherical Tokamak for Energy Production'. Accessed: Nov. 17, 2022. [Online]. Available: https://step.ukaea.uk/

[3] S. Orlandi, 'ITER Project: International Cooperation and Energy Investment', *Springer Proceedings in Physics*, vol. 243, pp. 169–191, 2020, doi: 10.1007/978-3-030-42913-3_26.

[4] S. Orlandi, 'ITER Project: International Cooperation and Energy Investment', *Springer Proceedings in Physics*, vol. 243, pp. 169–191, 2020, doi: 10.1007/978-3-030-42913-3_26.

[5] P. Kite and A. Richardson, 'The Promise of Nuclear Fusion', *PAM Review Energy Science & Technology*, vol. 1, no. 0, pp. 43–69, Aug. 2015, doi: 10.5130/pamr.v1i0.1385.

[6] Z. Cheng *et al.*, 'Irradiation effects in high-entropy alloys and their applications', *J Alloys Compd*, vol. 930, p. 166768, Jan. 2023, doi: 10.1016/J.JALLCOM.2022.166768.

[7] H. Watanabe, T. Tanaka, T. Turu, and Y. Kamada, 'Direct Observation of Cu Clusters and Dislocation Loops by Cs-Corrected STEM in Fe-0.6wt%Cu Alloy Irradiated in BR2', *Metals 2022, Vol. 12, Page 729*, vol. 12, no. 5, p. 729, Apr. 2022, doi: 10.3390/MET12050729.

[8] G. Janeschitz *et al.*, 'The ITER divertor concept', *Journal of Nuclear Materials*, vol. 220–222, pp. 73–88, Apr. 1995, doi: 10.1016/0022-3115(94)00447-1.

[9] M. Militzer, 'Phase field modelling of phase transformations in steels', *Phase Transformations in Steels*, pp. 405–432, Jan. 2012, doi: 10.1533/9780857096111.3.405.

[10] A. Choudhury, 'Phase-Field Modeling as a Method Relevant for Modeling Phase Transformation During Interdiffusion', *Handbook of Solid State Diffusion: Diffusion Fundamentals and Techniques: Volume 1*, vol. 1, pp. 363–389, Jan. 2017, doi: 10.1016/B978-0-12-804287-8.00007-5.

[11] R. Lai, D. He, G. He, J. Lin, and Y. Sun, 'Study of the Microstructure Evolution and Properties Response of a Friction-Stir-Welded Copper-Chromium-Zirconium Alloy', *Metals 2017, Vol. 7, Page 381*, vol. 7, no. 9, p. 381, Sep. 2017, doi: 10.3390/MET7090381.

[12] A. J. Cackett, J. J. H. Lim, P. Klupś, A. J. Bushby, and C. D. Hardie, 'Using spherical indentation to measure the strength of copper-chromium-zirconium', *Journal of Nuclear Materials*, vol. 511, pp. 610–616, Dec. 2018, doi: 10.1016/J.JNUCMAT.2018.04.012.

[13] S. A. Fabritsiev, S. J. Zinkle, and B. N. Singh, 'Evaluation of copper alloys for fusion reactor divertor and first wall components', *Journal of Nuclear Materials*, vol. 233–237, no. PART 1, pp. 127–137, Oct. 1996, doi: 10.1016/S0022-3115(96)00091-8.

[14] I. S. Batra, G. K. Dey, U. D. Kulkarni, and S. Banerjee, 'Microstructure and properties of a Cu–Cr–Zr alloy', *Journal of Nuclear Materials*, vol. 299, no. 2, pp. 91–100, Nov. 2001, doi: 10.1016/S0022-3115(01)00691-2.

[15] N. U. Obeyesekere, 'Pitting corrosion', *Trends in Oil and Gas Corrosion Research and Technologies: Production and Transmission*, pp. 215–248, Jan. 2017, doi: 10.1016/B978-0-08-101105-8.00009-7.

[16] S. A. Umoren, M. M. Solomon, and V. S. Saji, 'Basic concepts of corrosion', *Polymeric Materials in Corrosion Inhibition*, pp. 83–102, Jan. 2022, doi: 10.1016/B978-0-12-823854-7.00018-7.

[17] 'Tafel equation - Wikipedia'. Accessed: Jan. 25, 2023. [Online]. Available: https://en.wikipedia.org/wiki/Tafel_equation

[18] R. Bard, Allen J.; Faulkner, Larry, 'Electrochemical Methods: Fundmanentals and Applications', *ELECTROCHEMICAL METHODS Fundmanentals and Applications*, pp. 1–833, 2001.

[19] 'Griffith's Energy Release Rate'. Accessed: Jan. 25, 2023. [Online]. Available: https://www.fracturemechanics.org/griffith.html

[20] 'Pitting Corrosion'. Accessed: May 10, 2023. [Online]. Available: https://www.comsol.com/model/pitting-corrosion-100101

[21] 'Material Datasheet CuCrZr'.

[22] 'Tafel curve of copper electrode'. Accessed: Feb. 25, 2023. [Online]. Available: https://www.doitpoms.ac.uk/tlplib/batteries/Tafel_copper.php

[23] 'Copper - Element information, properties and uses | Periodic Table'. Accessed: Feb. 08, 2023. [Online]. Available: https://www.rsc.org/periodic-table/element/29/copper

[24] P. Ostachowski, W. Bochniak, M. Łagoda, and S. Ziółkiewicz, 'Strength properties and structure of CuCrZr alloy subjected to low-temperature KOBO extrusion and heat treatment', *International Journal of Advanced Manufacturing Technology*, vol. 105, no. 12, pp. 5023–5044, Dec. 2019, doi: 10.1007/S00170-019-04602-4/FIGURES/24.

[25] 'CuCr1Zr'. Accessed: Nov. 17, 2022. [Online]. Available: http://www.conductivity-app.org/alloy-sheet/19

[26] 'Table of Diffusion Coefficients'. Accessed: May 10, 2023. [Online]. Available: https://www.aqion.de/site/diffusion-coefficients

[27] 'Brittle Fracture of a Holed Plate'. Accessed: May 10, 2023. [Online]. Available: https://www.comsol.com/model/brittle-fracture-of-a-holed-plate-89321

[28] X. Bonnin *et al.*, 'ITER divertor plasma response to time-dependent impurity injection', *Nuclear Materials and Energy*, vol. 12, pp. 1100–1105, Aug. 2017, doi: 10.1016/J.NME.2017.03.010.